Anal. Chem. **2008,** *80,* 1891−1901

Electric-Field Control of the Tautomerization and Metal Ion Binding Reactivity of 8-Hydroxyquinoline Immobilized to an Electrode Surface

Vanessa Oklejas, Rory H. Uibel, Robert Horton, and Joel M. Harris*

Department of Chemistry, University of Utah, 315 South 1400, East Salt Lake City, Utah 84112-0850

Surface-enhanced Raman scattering (SERS) spectra of a metal-complexing ligand, immobilized to a silver electrode surface, exhibits significant structural changes upon application of modest potentials. A detailed spectroscopic investigation shows that the potential applied to the electrode surface governs the tautomerization equilibrium of the immobilized ligand, *p*-((8-hydroxyquinoline)azo)-benzenethiol (SHQ). Potential-dependent SERS spectra reveal that SHQ exists predominantly in a keto−hydrazone tautomeric form at applied potentials that are negative of −300 mV (vs Ag/AgCl), while the enol−azo tautomer is strongly favored at potentials positive of this value. The observed switching of the tautomer population occurs within a narrow range of applied potentials, ∼200 mV (Ag/AgCl). Electrical control over the tautomerization equilibrium of immobilized SHQ governs the reactivity of the ligand toward metal ion complexation, where the enol−azo tautomer exhibits much greater affinity for metal ion binding compared to its keto−hydrazone counterpart. Accordingly, the potential applied to the electrode can be used to influence metal ion binding of immobilized SHQ through control over the tautomerization equilibrium, to produce an electrically switchable surface for metal ion complexation. Large differences in the electric dipole moment of the two tautomers, estimated from density functional theory calculations, suggested a model where the potential dependence arises from the interaction of the ligand dipole with electric fields that exist at a polarized electrode surface. This model accurately predicts the relative tautomer populations versus applied potential, at interfacial electric fields that are consistent with previous measurements of the vibrational Stark effect at polarized interfaces. Potential applications of this technology to several areas of analytical chemistry are considered.

Polarized electrode surfaces produce large interfacial electric fields, which can influence the structure and reactivity of molecules at the electrode/solution interface, even in the double-layer charging region in the absence of faradaic (electron-transfer) processes. The effects of interfacial fields on molecules bound to metal surfaces are fundamental to controlling the switching behavior of molecular electronic devices.[1,2] Other molecular switches, in which structural (isomerization) changes to a surface-bound molecule can be reversibly triggered via a local electric-field stimulus, have been the focus of recent studies.[3,4] Likewise, the application of surface potentials can be used to manipulate the orientation and/or organization of adsorbed or bound molecules, including small, dipolar adsorbates,[5,6] immobilized DNA oligomers,[7−9] carboxylate-terminated *n*-alkanethiols,[10,11] and poly(hydroxyethyl methacrylate) thin films grafted onto gold surfaces.[12]

A number of studies employ controlled surface potentials to manipulate interfacial processes in chemical separations, demonstrating that the use of applied potential to modulate interfacial chemistry has immediate practical applications in analytical chemistry. Porter and co-workers[13−15] have developed electrochemically modulated chromatography, where the application of a potential to a conductive stationary phase, such as porous carbon, controls the free energy and retention of charged solute molecules at the graphitic surface. The control of ion transport by the application of applied potentials between nanometer pores connecting microfluidic channels has been demonstrated by Bohn et al.,[16,17] where the interfacial potential extends into the pore

* To whom correspondence should be addressed. E-mail: harrisj@chem.utah.edu.

(1) Gimzewski, J. K.; Joachim, C. *Science* **1999**, *283*, 1683−1688.
(2) Donhauser, Z. J.; Mantooth, B. A.; Kelly, K. F.; Bumm, L. A.; Monnell, J. D.; Stapleton, J. J.; Price, D. W. Jr. Rawlett, A. M.; Allara, D. L.; Tour, J. M.; Weiss, P. S. *Science* **2001**, *292*, 2303−2307.
(3) Alemani, M.; Peters, M. V.; Hecht, S.; Rieder, K.-H.; Moresco, F.; Grill, L. *J. Am. Chem. Soc.* **2006**, 128, 14446−14447.
(4) Henzl, J.; Mehlhorn, M.; Gawronski, H.; Rieder, K.-H.; Morgenstern, K. *Angew. Chem., Int. Ed.* **2006**, *45*, 603−606.
(5) Parry, D. B.; Harris, J. M.; Ashley, K. *Langmuir* **1990**, *6*, 209−217.
(6) He, G.; Xu, Z. *J. Phys. Chem. B* **1997**, *101*, 2101−2104.
(7) Kelley, S. O.; Barton, J. K.; Jackson, N. M.; McPherson, L. D.; Potter, A. B.; Spain, E. M.; Allen, M. J.; Hill, M. G. *Langmuir* **1998**, *14*, 6781−6784.
(8) Ceres, D. M.; Barton, J. K. *J. Am. Chem. Soc.* **2003**, *125*, 14964−14965.
(9) Yang, X.; Wang, Q.; Wang, K.; Tan, W.; Yao, J.; Li, H. *Langmuir* **2006**, *22*, 5654−5659.
(10) Lahann, J.; Mitragotri, S.; Tran, T. N.; Kaido, H.; Sundaram, J.; Choi, I. S.; Hoffer, S.; Somorjai, G. A.; Langer, R. *Science* **2003**, *299*, 371−374.
(11) Liu, Y.; Mu, L.; Liu, B. H.; Zhang, S.; Yang, P. Y.; Kong, J. L. *Chem. Commun.* **2004**, 1194−1195.
(12) Lokuge, I. S.; Bohn, P. W. *Langmuir* **2005**, *21*, 1979−1985.
(13) Deinhammer, R. S.; Ting, E.-Y.; Porter, M. D. *Anal. Chem.* **1995**, *67*, 237−246.
(14) Ting, E.-Y.; Porter, M. D. *Anal. Chem.* **1998**, *70*, 94−99.
(15) Keller, D. W.; Porter, M. D. *Anal. Chem.* **2005**, *77*, 7399−7407.
(16) Fa, K.; Tulock, J. J.; Sweedler, J. V.; Bohn, P. W. *J. Am. Chem. Soc.* **2005**, *127*, 13928−13933.
(17) Gatimu, E. N.; King, T. L.; Sweedler, J. V.; Bohn, P. W. *Biomicrofluidics* **2007**, *1*, 021502, 1−11.

10.1021/ac701808z CCC: $40.75
Published on Web 02/16/2008

because the Debye length is on the order of the pore diameter. Applying potentials to carboxylate-terminated *n*-alkanethiol-modified gold surfaces has been used to control the water contact angle and hence wettability of the surface[10] to achieve selective protein adsorption to the switchable interface.[11]

Nonfaradaic chemical reactions can also be controlled at electrode surfaces through the application of controlled potentials. An early, pioneering spectroelectrochemistry experiment demonstrated the influence of interfacial electric fields on the protonation equilibrium of an azo dye adsorbed to a platinum electrode.[18] The results were related to dependence of the interfacial proton activity on the applied potential, as well as the influence of the local electric field on the electronic structure of the dye molecule (electronic Stark effect). More recent studies have examined the influence of applied potential on the protonation equilibria of acid−base ligands thiol-bound to gold surfaces,[19−21] investigated by interfacial capacitance and electrochemical impedance measurements. The effects of a potential applied across immiscible liquid/liquid interfaces on the proton-transfer equilibria and interfacial excess concentration of weak acid surfactant molecules have been characterized by second-harmonic generation.[22] In a ligand-binding example that is not based on proton transfer, application of repulsive (negative) potentials has been shown to influence the stability of DNA duplexes formed to surface-immobilized ssDNA, which could control the sensitivity of hybridization to base pair mismatches.[23] Potential control has been used in a selective sorption-based spectroelectrochemical sensor to modulate the analyte optical response, either absorption[24] or fluorescence.[25] Finally, an immobilized poly(L-cysteine) layer was controlled for metal ion binding by varying of the redox state of the cysteine ligands under potential control at glassy carbon electrodes.[26]

In the present work, several of the above concepts are employed to produce a reversible metal ion binding surface that can be manipulated at modest potentials, in the absence of faradaic processes. To achieve this result, a well-characterized ligand for metal ion complexation, 8-hydroxyquinoline, was immobilized to a silver electrode via an azo−(phenyl)−thiol linker. Surface-enhanced Raman scattering (SERS) spectra of this ligand, measured as a function the potential applied to the electrode, demonstrated that the ligand can be reversibly "switched" between two tautomeric forms, analogous to electric-field induced isomerization of immobilized ligands recently reported.[3,4] The tautomerization equilibrium was also influenced by the presence of metal ions (Cu^{2+}), which bind strongly to the azo−quinoline tautomer but not detectably to the keto−hydrazone form. The coupling of metal ion complexation equilibrium to the potential-dependent tautomeric state of the ligand, therefore, forms the basis for control of the binding of metal ions to the hydroxyquinoline-modified electrode surface, analogous to redox-state switching recently reported.[26] The potential-dependent switching of the hydroxyquinoline ligand was consistent with the difference in stability of the two tautomers in the electric field of the double layer, based on large differences in their electric dipole moments predicted by density functional theory. The results suggest a new paradigm for electrical control over interfacial reactions: controlled tautomerization of immobilized ligands provides a facile method for introducing reversible electronic and molecular structural differences that could be exploited to produce an electrically "switchable" surface for a variety of analytical chemistry applications. Surface-enhanced Raman spectroscopy provides critical information about changes in the structure of ligands bound to metal surfaces, under the control of the applied potential.

EXPERIMENTAL SECTION

Synthesis of *p*-([8-Hydroxyquinoline]azo)benzenethiol (SHQ). The thiol-anchored ligand, SHQ, was synthesized based upon a procedure developed by Marshall and Mottola[27,28] for preparing an analogous silane-bound 8HQ for silica surfaces. In a 5-dram glass vial, 4-aminothiophenol (Aldrich), 60.0 mg, 0.48 mmol, was predissolved in MeOH and then combined with 5 mL of 0.1 M HCl. In a second 5-dram vial, 8-hydroxyquinoline (Aldrich), 96.1 mg, 0.66 mmol, was also predissolved in MeOH and then combined with 5 mL of 0.1 M HCl. The two vials were sonicated (Sonicor Instruments Corp.; model: SC-40) until clarity (15−20 min). The two reagents were combined in a 50-mL round-bottom flask. Sodium nitrite (50.3 mg, 0.73 mmol), dissolved in 0.5 mL of ddH_2O, was added to the reagents in the round-bottom flask to form SHQ; see Figure 1. The reaction stirred overnight at room temperature.

The reaction mixture was added to 100 mL of $CHCl_3$ in a separatory funnel and washed three times with 100 mL of ddH_2O. Concentrated hydrochloric acid was added to the ddH_20 in the separatory funnel to move the SHQ from the organic to the aqueous layer. The aqueous layer was then washed three times with 100 mL of $CHCl_3$ to remove excess starting material. Ammonium hydroxide was added dropwise until a neutral pH was reached based upon litmus paper. Near neutral pH, a precipitate formed that was collected on a fine frit filter and rinsed with 50 mL of 0.1 M NH_4OH. The SHQ was removed from the filter with ethanol and then stored at −20 °C. SHQ was also stored as a solid upon removal of the EtOH by rotary evaporation.

Electrospray ionization mass spectrometry (Micromass Quattro II) in positive ion mode was used to characterize the SHQ product from dilute formic acid in methanol. Initial results showed a major peak at $m/e = 282.0$, corresponding to the calculated m/e for protonated SHQ, $C_{15}H_{12}N_3OS$ (M + H) = 282.06. There was also evidence of disulfide-linked dimers, from a detectable intensity peak at 280.9 amu, which is likely a doubly charged, disulfide dimer of SHQ (ES^{2+} calculated for $C_{30}H_{22}N_3O_2S_2$ (M + 2H) 281.1); a minor peak at 405.0 amu (ES^+ calculated for $C_{21}H_{17}N_4OS_2$ (M + H) 405.08) was consistent with the disulfide formation between SHQ and the 4-aminothiophenol starting material. β-Mercapto-

(18) Schmidt, P. H.; Plieth, W. J. *Ber. Bunsenges. Phys. Chem.* **1987**, *91*, 323−329.
(19) Bryant, J. A.; Crooks, R. M. *Langmuir* **1993**, *9*, 385.
(20) Schweiss, R.; Pleul, D.; Simon, F.; Janke, A.; Welzel, P. B.; Voit, B.; Knoll, W.; Werner, C. *J. Phys. Chem. B* **2004**, *108*, 2910.
(21) Burgess, I.; Seivewright, B.; Lennox, R. B. *Langmuir* **2006**, *22*, 4420.
(22) Naujok, R. R.; Higgins, D. A.; Hanken, D. G.; Corn, R. M. *J. Chem. Soc., Faraday Trans.* **1995**, *91*, 1411.
(23) Heaton, R. J.; Peterson, A. W.; Georgiadis, R. M. *Proc. Natl. Acad. Sci. U.S.A.* **2001**, *98*, 3701.
(24) Shi, Y.; Slaterbeck, A. F.; Seliskar, C. J.; Heineman, W. R. *Anal. Chem.* **1997**, *69*, 3679.
(25) Kaval, N.; Seliskar, C. J.; Heineman, W. R. *Anal. Chem.* **2003**, *75*, 6334.
(26) Johnson, A. M.; Holcombe, J. A. *Anal. Chem.* **2005**, *77*, 30.
(27) Marshall, M. A.; Mottola, H. A. *Anal. Chem.* **1983**, *55*, 2089.
(28) Marshall, M. A.; Mottola, H. A. *Anal. Chem.* **1985**, *57*, 729.

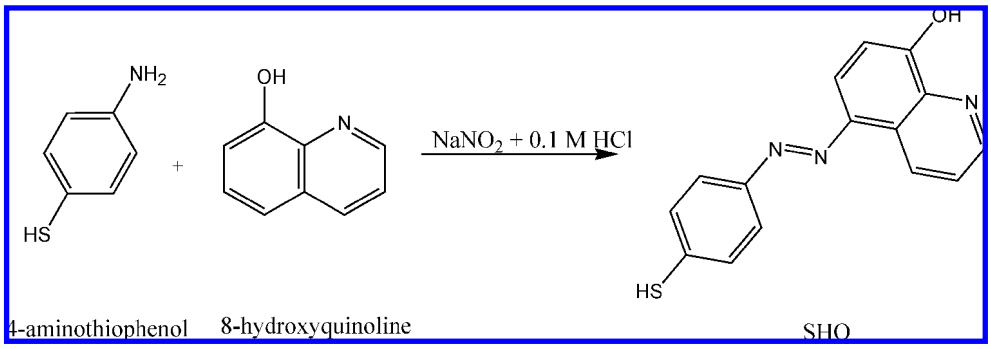

Figure 1. Synthesis of p-([8-hydroxyquinoline]azo)benzenethiol (SHQ).

ethanol (2−3 drops) was added to the solution to reduce the disulfides, resulting in the only a single peak from SHQ (ES^+ calculated for $C_{15}H_{12}N_3OS$ (M + H) 282.06, observed 282.0).

Substrate Preparation and SHQ Monolayer Assembly. Electrodes were constructed from 99.999% Ag rod (6.5-mm diameter, Alfa Aesar). All Ag surfaces were polished with 800-, 1500-, and 2000-grit silicon carbide paper (3M), followed by successive polishing with a series of alumina particle slurries (1.0−0.05 μm particle size) suspended on microfiber polishing cloth (Buehler), with a final polish on the wet polishing cloth free of alumina. The electrodes were then sonicated in ethanol for 15 min to facilitate removal of any traces of residual alumina. The polished Ag surfaces exhibited a surface roughness of 2.0 nm (rms), measured by atomic force microscopy. Previous work from this laboratory has shown that Ag surfaces polished in this manner exhibit a factor of ~10 times smaller enhancement compared with electrochemically (ORC) roughened surfaces; unlike ORC-roughened surfaces; however, potential-dependent SERS spectra acquired on the polished electrodes are reversible and reproducible even after negative potential excursions.[29] To form self-assembled monolayers (SAMs), freshly polished Ag electrodes surfaces were immersed in 1 mM SHQ in ethanol for ~12 h. Mixed monolayers containing SHQ and diluent thiol species, heptanethiol (95%, Aldrich) or mercaptohexanol (97%, Aldrich), were assembled from ethanol solutions containing 2 mM heptanethiol and 1 mM SHQ, and 7 mM mercaptohexanol and 1 mM SHQ, respectively.

Annealed Ag films were produced using a Veeco CVC CVE-20 filament evaporator (TFS Technologies, Albuquerque, NM). A base pressure between 8×10^{-7} and 2×10^{-6} Torr was maintained during Ag deposition using a combination of sorption and turbo pumps. Freshly cleaved muscovite mica substrates were positioned 23 cm above the Ag source. A Ti adhesion layer was deposited at ~2 Å/s rate by resistively heating Ti flake (99.99%, Alfa Aesar) in a Mo boat to achieve a film thickness of 5 nm. Ag shot (99.999% Alfa Aesar) was resistively heated in a separate Mo boat to deposit a 3-μm-thick Ag film at a rate of ~2 Å/s. Deposition rates and film thickness were monitored using a Kronos QM-311 thickness gauge. Immediately following deposition, the Ag films were annealed at 300 C for 4 h using backside illumination from two quartz lamps to produce a well-ordered surface.[30] After the lamps were turned off, the samples were allowed to cool to room temperature. The chamber was vented to atmosphere, and the samples were immediately immersed in an ethanol solution of 0.5 mM SHQ overnight and rinsed thoroughly with ethanol prior to use.

SHQ Monolayer Characterization. X-ray photoelectron spectroscopy was used to check the elemental composition of SHQ monolayers. X-ray photoelectron spectroscopy (VG Scientific 220i-XL) was performed using a monochromatic Al Kα X-ray source, hemispherical electron energy analyzer, with electron takeoff angles varied between 0° and 55°. High-resolution scans of the C_{1s}, N_{1s}, S_{2p}, O_{1s}, and Ag_{3d} spectral regions were acquired and confirmed the presence of the elements expected to arise from immobilized SHQ; no other elements were detected in survey scans. Angle-dependent XPS data showed a consistent decrease in the signals from silver and sulfur as the electron takeoff angles were increased from 0° to 55°. At higher takeoff angles, the surface selectivity of XPS photoemission increases due to the greater path length for electron scattering and energy loss at higher angles.[31] The relative intensity of photoemission from Ag and S dropped by −51 and −36%, respectively, as the takeoff angle was increased from 0° to 55° (see Supporting Information). Based on high-resolution scans, the signals from carbon, nitrogen, and oxygen, on the other hand, increase at higher takeoff angles, gaining 22, 10, and 28%, respectively, between 0° and 55°. The results are consistent with an oriented ligand sulfur-bound to silver (refer to Figure 1), where the oxygen, carbon, and nitrogen reside nearer the monolayer/vacuum interface and the silver and sulfur are covered.

The integrity of SHQ monolayers at a monolayer/solution interface was characterized by cyclic voltammetry. The electrochemical cell consisted of a one-compartment, three-electrode configuration employing a Ag/AgCl (saturated KCl) reference electrode and a coiled Pt wire (0.127-mm diameter × 1-m length, Alfa Aesar) counter electrode, and was controlled by a potentiostat (CV-27, Bio-analytical Systems). Cyclic voltammograms (CVs) were acquired from electrodes functionalized with SHQ and then immersed in acetate-buffered solution (pH 4.8) that had been purged with nitrogen. CVs of these electrodes were recorded in the presence and absence of Cu^{2+} ions in solution (see Supporting Information). The signals of all recorded CVs of SHQ-functionalized electrodes are dominated by charging current associated with the double layer. CVs performed in the absence of Cu^{2+} ions are featureless except for a very small, broad, reversible wave centered

(29) Oklejas, V.; Harris, J. M. *Appl. Spectrosc.* **2004**, *58*, 945−951.
(30) Baiker, A.; Grunwaldt, J.-D.; Atamny, F.; Gobel, U. *Appl. Surf. Sci.* **1996**, *99*, 353.
(31) Fadley, C. S. *J. Electron. Spectrosc.* **1974**, *5*, 725.

at roughly −0.2 V (vs Ag/AgCl); see Supporting Information. This small wave cannot be reasonably attributed to a faradaic process because the reduction potential of neither the azo nor quinoline groups occurs at potentials less negative than −1 V.[32−34] It is difficult to gather any conclusive information from such a small, broad wave. However, it should be noted that the position of the wave peak is coincident with a change in population of the tautomeric forms of immobilized SHQ observed with in situ SERS measurements (see below). A large difference in dipole moment between these two tautomeric forms is predicted by density functional theory calculations. Accordingly, it is possible that the small broad wave represents the movement of charge accompanying the change in dipole located close to the electrode surface.[35] For CVs performed in the presence of 0.6 mM $Cu(SO_4)$, a small reversible wave was observed ∼−0.45 V (vs Ag/AgCl). This wave is attributed to the reduction of the Cu^{2+}−SHQ complex, which has previously been reported to occur at −0.48 V (vs Ag/AgCl).[34] In contrast, a reduction potential for uncomplexed Cu^{2+} on bare Ag electrodes was observed at −0.12 V (vs Ag/AgCl) as expected. These results confirm that SHQ monolayers prevent Cu^{2+} ions from accessing the Ag electrode surface and are consistent with complete surface coverage by the ligand; this conclusion is supported by previous electrochemical results[33] showing that thiolated azobenzenes and ferrocenylazobenzenes form well-organized monolayers on gold surfaces.

SERS Spectroeletrochemical Measurements. A Pine RDE4 potentiostat was used to control the potential applied to the Ag electrode in a three-electrode configuration. All measurements were referenced to Ag/AgCl (saturated KCl) electrode, and a Pt wire (0.127-mm diameter × 1-m length, Alfa Aesar) was employed as the counter electrode. Excitation radiation for SERS was provided by a Lexel 95 Ar^+ laser operated at 514.5 nm. The excitation beam was brought to a focus with a power density of 50 mW/cm^2 at the electrode surface (∼300 μm × ∼500 μm elliptical spot size). The excitation beam was fixed at 55° with respect to the surface normal in the vertical plane, and scattered light was collected at 60° in the horizontal plane with an f/1.8 camera lens (JML Optics). The elastically scattered light was filtered from the signal with a holographic notch filter (Kaiser) before being focused by a second f/1.8 camera lens onto a fiber optic bundle. The fiber-optic cable, composed of ∼60 low-hydroxyl, 100-μm-diameter quartz fibers, was constructed in a spot-to-line configuration: the collected light, brought to a focus at the circular fiber-optic head, was transmitted by the fibers to a linear array of fibers at its output end. The resulting line-shaped image was focused onto a 110-μm entrance slit of an f/4 Spex monochromator (0.5-m focal length). The SERS signal was detected by a 256 × 1024 pixel CCD (Andor Technology) thermoelectrically cooled to −70 °C. Typical signal integration times were 5−15 s.

Despite the relative smoothness of highly polished electrode and annealed Ag surfaces, the intensities of the SERS signal collected were easily measurable, which indicates that there is an electronic resonance contribution to the surface-enhanced Raman scattering. This observation is consistent with the absorption band of SHQ that tails into the visible region, where the molar absorptivity in ethanol at 514.5 nm is ∼600 M^{-1} cm^{-1}. Also, $\pi-\pi$ interactions between planar aromatic moieties within SAMs have been shown to cause substantial red-shifting and band broadening in electronic absorption spectra,[32] which further explains the ample SERS signal observed from SHQ at smooth Ag surfaces.

All spectroelectrochemical measurements were performed in buffered solutions with 25 mM buffer salts, 20 mM NaCl, x mM $Cu(SO_4)$, and (90 mM − 4X) $NaClO_4$, where concentration of the $NaClO_4$ was adjusted to maintain constant ionic strength with varying Cu^{2+} concentrations. The concentration of $Cu(SO_4)$ in solution ranged from 0 to 30 mM. Three different buffer salts were used to control pH over several ranges: chloroacetate/chloroacetic acid (pK_a = 2.88), acetate/acetic acid (pK_a = 4.76), and monohydrogen phosphate/phosphate (pK_a = 12.15). The pH of the buffered solution was adjusted using $HClO_4$ to levels appropriate to each buffer system (e.g., pH 2.4 for chloroacetate, pH 4.8 for acetate, and pH 12.1 for phosphate-buffered solutions).

RESULTS AND DISCUSSION

SERS Spectra of SHQ-Modified Electrode Surfaces. Previous Raman spectroscopic studies of an analogous immobilized ligand, 5-(*p*-trimethoxysilylphenylazo)-8-hydroxyquinoline (SiHQ), immobilized on silica surfaces have shown that the 8HQ moiety undergoes two proton-transfer steps: from the protonated to neutral form (pK_{a1} ∼ 2.7) and from a neutral to an anionic form (pK_{a2} ∼ 8.6).[36−38] The Raman spectra of the silica immobilized ligand are consistent with pH-dependent changes in tautomerization of 8-hydroxyquinoline, where at low pH conditions the protonated keto−hydrazone tautomer is the dominant form while, at high pH, the deprotonated enol−azo tautomer is prevalent, and at intermediate pH values, the neutral ligand is an equilibrium of both tautomeric forms;[36,37,39,40] see Figure 2. Raman spectra of silica immobilized SiHQ exposed to solutions containing millimolar concentrations of Cu^{2+} indicate that metal ion complexation occurs exclusively with the azo−quinoline (enol−azo) tautomeric form,[36,37,41] which is consistent with much stronger complexation by the phenolic oxygen compared to a ketone.

SERS spectra of the SHQ ligand immobilized on Ag were acquired in solutions with varying pH and [Cu^{2+}] in order to identify spectral features associated with the two tautomeric forms of the immobilized ligand. (Figure 3 and Table 1). SERS spectra of SHQ immobilized at Ag electrode surfaces are very similar to Raman spectra reported previously for SiHQ.[36,37] These strong spectral similarities indicate that the structure of the chelating moiety of SHQ is minimally perturbed by the change in anchoring group from silanol to thiol (see below). The SERS bands associated with SHQ-modified electrodes under all three pH conditions and in the presence of Cu^{2+} are listed and assigned in Table 1. The salient spectral features include the ν(C=C)$_{phenyl}$ mode (1580 cm^{-1}) and the ν(C=C)$_{quinoline}$, ν(C=N), and ν(N=N) modes associated with the azo−quinoline and keto−hydrazone groups

(32) Caldwell, W. B.; Chen, K.; Herr, B. R.; Mirkin, C. A.; Hulteen, J. C.; Van Duyne, R. P. *Langmuir* **1994**, *10*, 4109.
(33) Herr, B. R.; Mirkin, C. A. *J. Am. Chem. Soc.* **1994**, *116*, 1157.
(34) Garay, F.; Solis, V.; Lovrić, M. *J. Electroanal. Chem.* **1999**, *478*, 17.
(35) Goa, X.; White, H. S.; Chen, S.; Abruña, H. D. *Langmuir* **1995**, *11*, 4554.
(36) Uibel, R. H.; Harris, J. M. *Appl. Spectrosc.* **2000**, *54*, 1868.
(37) Uibel, R. H.; Harris, J. M. *Anal. Chem.* **2002**, *74*, 5112.
(38) Kolstad, A. K.; Chow, P. Y. T.; Cantwell, F. F. *Anal. Chem.* **1988**, *60*, 1565.
(39) Sett, P.; Paul, N.; Brahma, S. K.; Chattopadhyay, S. J. *J. Raman Spectrosc.* **1999**, *30*, 611.
(40) Trotter, P. J. *Appl. Spectrosc.* **1977**, *31*, 30.
(41) Jezorek, J. R.; Freiser, H. *Anal. Chem.* **1979**, *51*, 366.

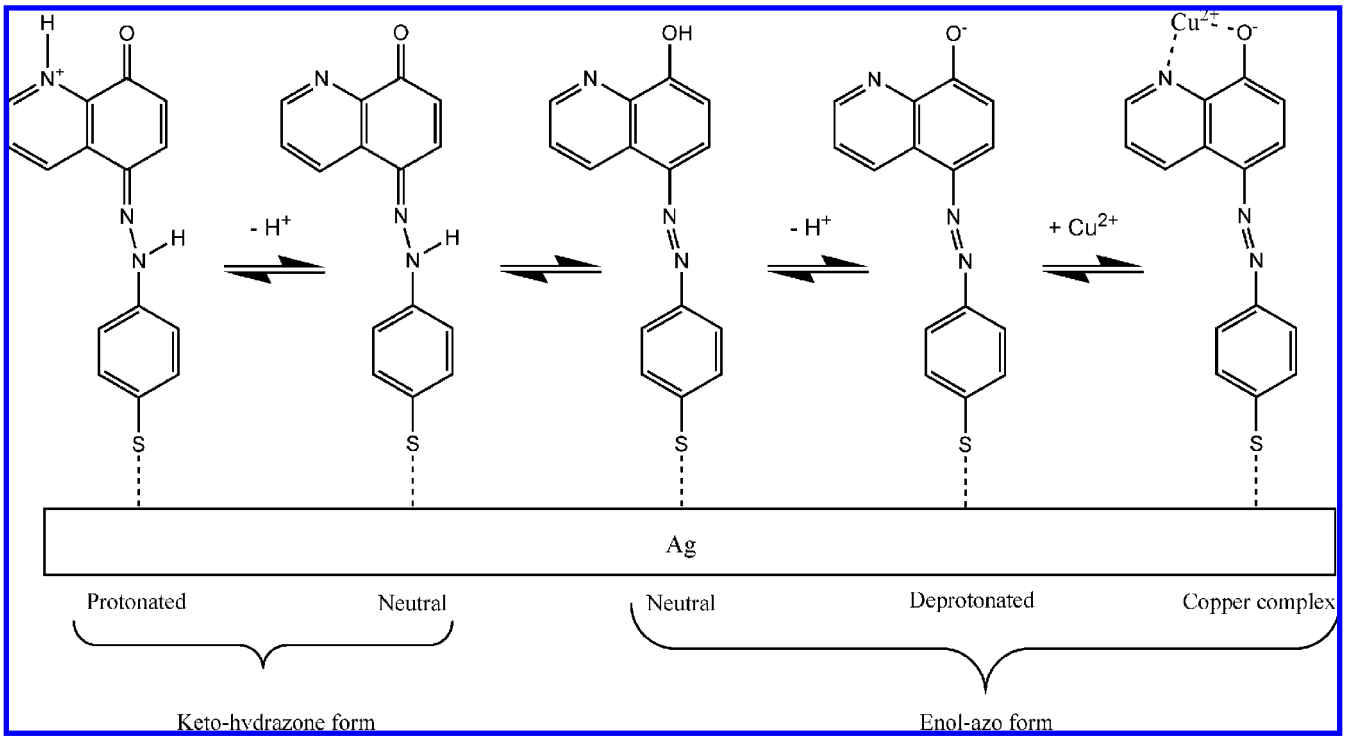

Figure 2. Tautomeric forms of p-([8-hydroxyquinoline]azo)benzenethiol (SHQ).

Table 1. Band Assignment of SERS Spectrum of SHQ Immobilized at Ag Electrode[a].

pH 2.4	pH 4.8	pH 12.1	30 mM Cu^{2+}	assignment
1646 s				ν(C=O)
1586 s	1579 m	1579 m	1580 m	ν(C=C)$_{\text{phenyl ring}}$
1437 w	1427 m	1437 vs	1430 m	ν(N=N); ν(C=C)$_{\text{quinoline}}$
1396 m	1392 s	1394 s	1393 m	ν(C=N); ν(C=C)$_{\text{quinoline}}$
1372 w	1375 s	1371 m,sh	1370 s	napthalenic sym str. (a)
	1333 m		1332 m	ν(C=C); ν(C=N)
	1305 w	1306 w	1304 w	δ_{rock}(C−H);
1189 w	1193 m	1193 m	1193 m	ν(C−N)
	1158 w		1158 w	δ_{bend}(C−H); n (C−N)
1144 w	1138 m	1146 s	1138 m	δ_{bend}(C−H) - n (C−N=)
1079 m	1079 w	1080 m	1079 w	ring breathing
1006 w	1006 w	1006 w	1006 w	ring breathing

[a] Trotter, P. J. *Appl. Spectrosc.* **1977**, *31*, 30. s strong; m medium; w weak; sh shoulder.

(1390−1440 cm^{-1}).[40] A cluster of frequencies located between 1350 and 1300 $cm^{-1}$are assigned to the pyridyl ring within the quinoline moiety of SHQ. These SERS spectra reflect structural changes that occur in immobilized SHQ upon changes in pH or coordination to Cu^{2+}, where either the enol−azo tautomeric form is favored (high pH and high [Cu^{2+}]) or the keto−hydrazone form is favored (low pH). The most noticeable spectral feature is the band located at 1642 cm^{-1}, which appears at low pH and is readily assigned to the carbonyl-stretching mode, ν(C=O), associated with the keto−hydrazone tautomer.[36,37,39,40] This band appears to be the only band that is both unambiguously assigned to a specific tautomeric form and is well resolved from other vibrational modes. These observations all support the conclusion that SHQ, immobilized by a thiol linkage to Ag surfaces, reacts with Cu^{2+} ion as the enol−azo tautomer, where the ligand structure and interfacial reactivity are consistent with silane-tethered 8HQ immobilized onto silica surfaces.

Potential Dependence of SERS Spectra of Immobilized SHQ. SERS spectra were acquired under potential control to investigate the effects of applied potential on the structure of immobilized SHQ and its reactivity toward Cu^{2+} ions; see Figure 4. SERS spectra show that applied potential influences the structure of SHQ on Ag electrode surfaces immersed in mildly acidic, buffered solution (pH 4.8). Changes in spectra as a function of applied potential do not arise from faradaic processes; the voltammetric response shows no detectable redox activity exceeding the charging current (see above). This is a reasonable conclusion because neither oxidation nor reduction of the azo or hydroxyquinoline groups occurs within the range of potentials that are applied in these experiments.[34] Furthermore, the observed potential dependence in Figure 4 is not associated with restructuring of the Ag surface or the electronic properties of SERS-active sites on the mechanically polished Ag electrode surfaces. Raman scattering collected from SHQ immobilized on well-ordered Ag

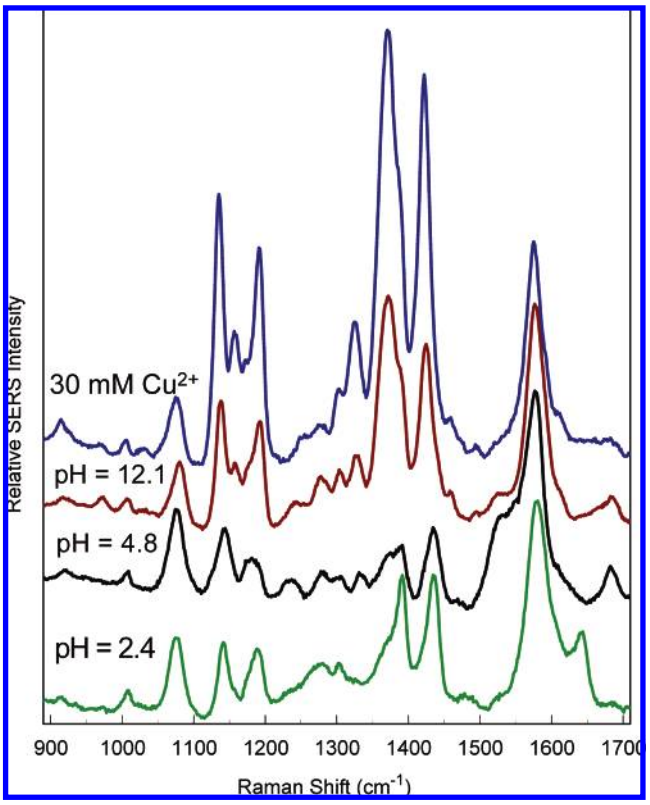

Figure 3. In situ SERS spectra of SHQ immobilized at Ag electrode surfaces at open circuit. From bottom to top: pH 2.4 (green line); pH 4.8 (black line); pH 12.1 (red line); and acetate-buffered solution pH 4.8, containing 30 mM $Cu(SO_4)$ (blue line). SERS spectra were background subtracted and scaled to the ν(C═C) stretching mode at 1580 cm^{-1} for comparison.

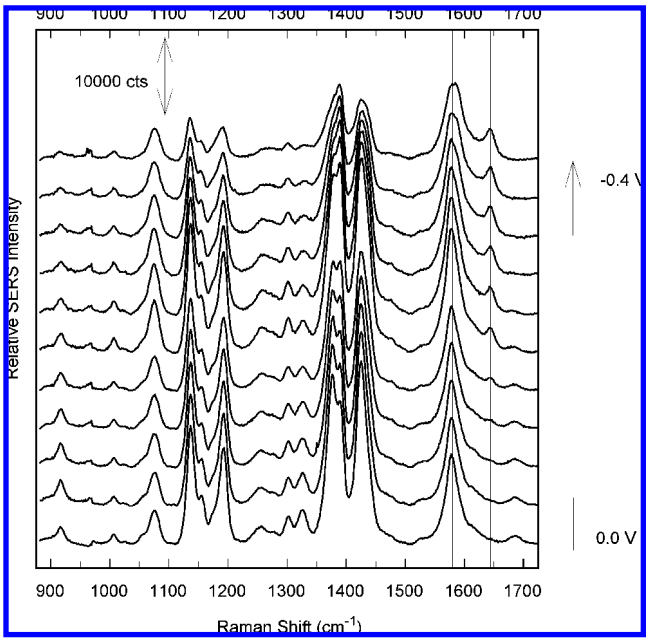

Figure 4. In situ SERS spectra of SHQ immobilized at highly polished Ag electrode surfaces as a function of applied potential (V vs Ag/AgCl). These spectra were background subtracted and offset for plotting, but are not normalized. The unique ν(C═O) peak at 1642 cm^{-1} from the keto−hydrazone tautomer is noted, along with the ν(C═C) at 1580 cm^{-1}, which remains constant with changes in the tautomer populations.

films vapor deposited on freshly cleaved mica and annealed, which is predominantly Ag_{111} and contains few surface defects,[30] produces equivalent spectra and potential dependence (see Supporting Information).

The variation in the SERS spectra of immobilized SHQ is consistent with a potential-dependent change in the relative surface population of SHQ tautomers. The increasing intensity of the ν(C═O) band at 1642 cm^{-1} provides clear evidence that the population of the keto−hydrazone tautomer of SHQ grows with increasingly negative applied potentials. The corresponding decrease in the enol−azo tautomer is further supported by the decreasing intensity of the ν(N═N) band, at ∼1435 cm^{-1}, which is associated with the azo functional group of this tautomer. The observed potential-dependent spectral changes are reversible over a period of hours. It is important to note the similarities in the spectra of Figure 3 with those in Figure 4. For example, comparison of spectrum of immobilized SHQ acquired at open circuit at very low pH, where the keto−hydrazone tautomer is strongly favored due to protonation of the ligand,[36,37] is nearly identical to the spectrum obtained at −0.4 V (vs Ag/AgCl) in mildly acidic (pH 4.8) solution. Similarly, at 0.0 V (vs Ag/AgCl), the spectrum of the ligand corresponds to the enol−azo form and is very similar to the spectra observed at open circuit under strongly basic conditions (pH 12.1), where the enol−azo form is dominant.[37] The sensitive potential dependence of the tautomerization is only observed in the intermediate pH region (pH 4.8), where the neutral form of the ligand dominates. In highly basic (pH 12.1) or acidic (pH 2.4) conditions, the tautomerization equilibrium overwhelmingly favors the enol−azo and keto−hydrazone forms, respectively, and could not be manipulated with changes in applied potential.

To estimate the fractional population of the keto−hydrazone relative to the total ligand population, the ratio of peak intensities from ν(C═O) at 1642 cm^{-1} from this tautomer, relative to ν(C═C) at 1580 cm^{-1}, was plotted as a function of applied potential (top curve in Figure 5). The $\nu_{C=C}$ mode was chosen as a reference because its intensity is stable as a function of potential. This stability is apparent in the spectra in Figure 4, which are not normalized. The 1079-cm^{-1} ring mode was also tested as a reference band, and the results obtained were equivalent. From the data in Figure 5, it is clear that the intensity of the ν(C═O) relative to the ν(C═C) band increases from undetectable values to maximum values within a narrow potential window centered at ∼−200 mV (vs Ag/AgCl). Potential steps more negative than −300 mV do not result in further increases in the ratio of $I_{\nu(C=O)}/I_{\nu(C=C)}$. The intensity ratios were normalized to the largest value in the plot, where the tautomeric conversion is assumed to be saturated since no subsequent structural changes occur beyond this range.

Metal Ion Binding to Immobilized SHQ. As introduced above, the Raman spectra of SHQ are also influenced by the presence of metal ions that complex with the azo−quinoline (enol−azo) form of the immobilized ligand. Upon addition of Cu^{2+} (see Figure 6), the SERS spectra show changes in the ν(C═N) band associated with the quinoline ring, near 1330 cm^{-1}, that reflect differences in the structure of the ligand upon metal ion complexation. As the Cu^{2+} concentration increases, the SERS intensity of the ν(C═O) band at 1642 cm^{-1} steadily decreases,

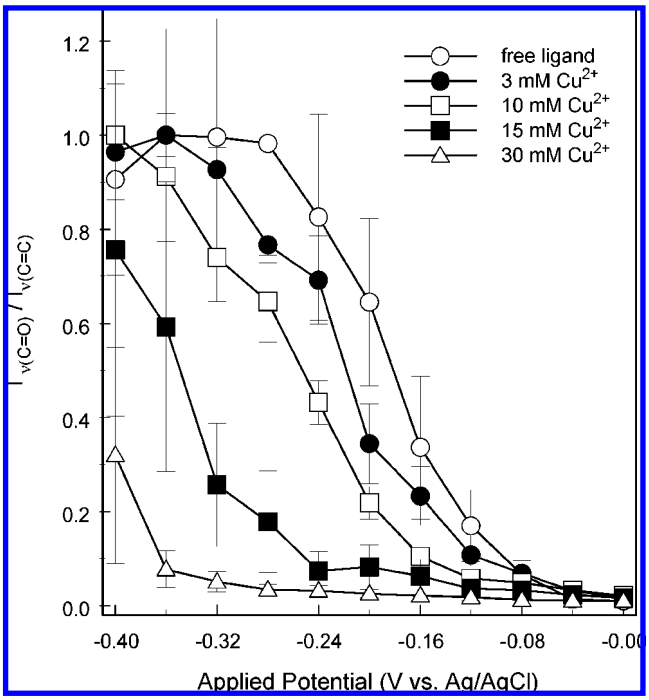

Figure 5. Relative population of keto−hydrazone tautomer of immobilized SHQ ($I_{\nu(C=O)}/I_{\nu(C=C)}$) as a function of applied potential (V vs Ag/AgCl) in solutions with varying [Cu^{2+}].

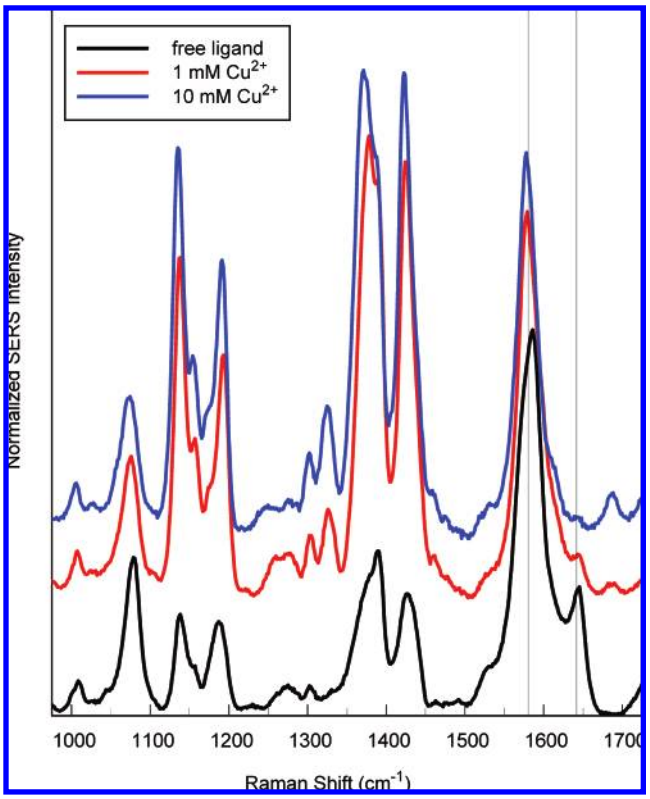

Figure 6. In situ SERS spectra of SHQ immobilized at highly polished Ag electrode surfaces as a function of [Cu^{2+}] in acetate-buffered solution (pH 4.8) at −0.24 V (vs Ag/AgCl). SERS spectra were background subtracted and normalized relative to the highlighted ν(C=C) stretching mode at 1580 cm^{-1}; note changes in the keto−hydrozone population from variation in the ν(C=O) peak at 1642 cm^{-1}.

while SERS intensities of bands associated with ν(C=N) and ν(N=N) modes, at ~1390 and 1430 cm^{-1}, rise. This trend is consistent the enol−azo tautomer exhibiting much higher affinity for Cu^{2+} relative to its keto−hydrazone counterpart. The effect of metal ion binding on the ligand tautomerization can be seen in Figure 5, where increasing [Cu^{2+}] lowers the fraction of the keto−hydrazone from ($I_{\nu(C=O)}/I_{\nu(C=C)}$) at any applied potential. At sufficiently high [Cu^{2+}], the applied potential can no longer modulate the tautomeric equilibrium as metal ion complexation overwhelming favors enol−azo tautomer. The data are consistent with Cu^{2+} complexation to the enol−azo tautomer, which depletes the population of the keto−hydrazone tautomer according to the following coupled equilibria:

$$Hy \xleftrightarrow{K_{taut}} HQ \quad (1)$$

$$HQ \xleftrightarrow{K_{A2}} Q^- + H^+ \quad (2)$$

$$Q^- + Cu^{2+} \xleftrightarrow{K_{bind}} CuQ^+ \quad (3)$$

where Hy is the neutral keto−hydrazone tautomer, HQ is the neutral azo−quinoline form, Q^- is the deprotonated quinolate, and CuQ^+ is the metal ion bound complex; see structures in Figure 2.

To account for the effect of metal ion concentration on the tautomer populations, an expression describing the relative fractions of the two different tautomers can be developed from the coupled equilibria in eqs 1−3. The ratio of the populations of neutral enol−azo (hydroxyquinoline) to keto−hydrazone tautomers is given by the tautomerization equilibrium constant: $[HQ]/[Hy] = K_{taut}$, the deprotonated quinolate fraction depends on the interfacial proton activity a_{H^+}, $[Q^-]/[HQ] = K_{A2}/a_{H^+}$, and the Cu^{2+}-bound fraction of the quinolate tautomer is determined by the Cu^{2+} binding equilibrium, $[CuQ^+]/[Q^-] = K_{bind}a_{Cu^{2+}}$, where $a_{Cu^{2+}}$ is the interfacial activity of Cu^{2+}. Combining these coupled equilibria, the keto−hydrazone fraction can be expressed as

$$\frac{[Hy]}{[Hy] + [HQ] + [Q^-] + [CuQ^+]} = \frac{1}{1 + K_{taut} + K_{taut}K_{A2}/a_{H^+} + K_{taut}K_{A2}K_{bind}a_{Cu^{2+}}/a_{H^+}} \quad (4)$$

where, at the interfacial pH of these experiments, the protonated hydrazone fraction is negligible.

This model for the speciation of the immobilized ligand was used to fit the Cu^{2+} concentration dependence of the observed hydrazone fraction at each of the applied potentials; see example in Figure 7. To reduce the number of parameters in the fit, the binding constant of the ligand for forming the Cu^{2+} complex (K_{bind} ~ 5×10^8) and the second acid dissociation constant, $K_{A2} \sim 2.5 \times 10^{-9}$, were taken from measurements on the equivalent silane-derivatized ligand immobilized to silica, corrected for minor surface charging determined from measured zeta-potentials.[37] The validity of this silane-immobilized ligand to predict the acid−base and complexation chemistry of the thiol-immobilized ligand was supported by density functional theory calculations (B3LYP 6-31G-

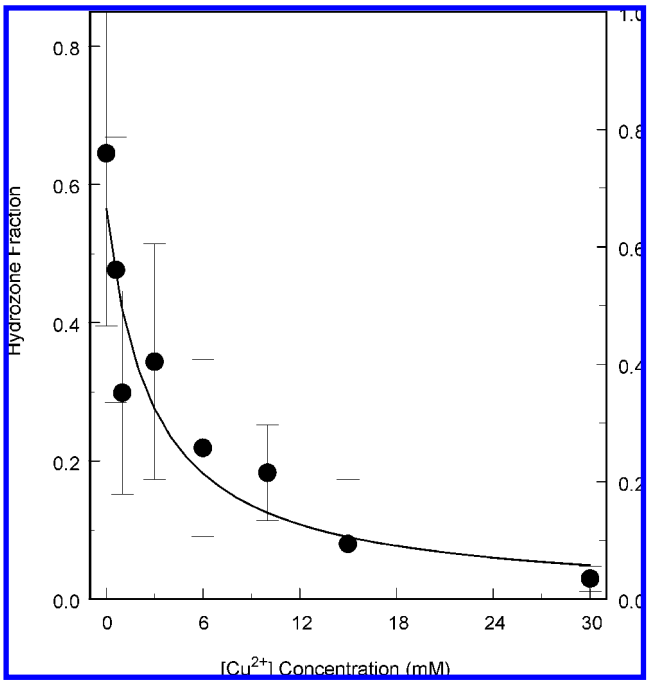

Figure 7. Plot of the relative population of keto−hydrazone tautomer of immobilized SHQ ($I_{\nu(C=O)}/I_{\nu(C=C)}$) as a function of [$Cu^{2+}$] in solution. Experimental results are represented by symbols, and the best fit to eq 4 is presented as a solid line. Experimental results were obtained at −0.2 V (vs Ag/AgCl) at pH 4.8.

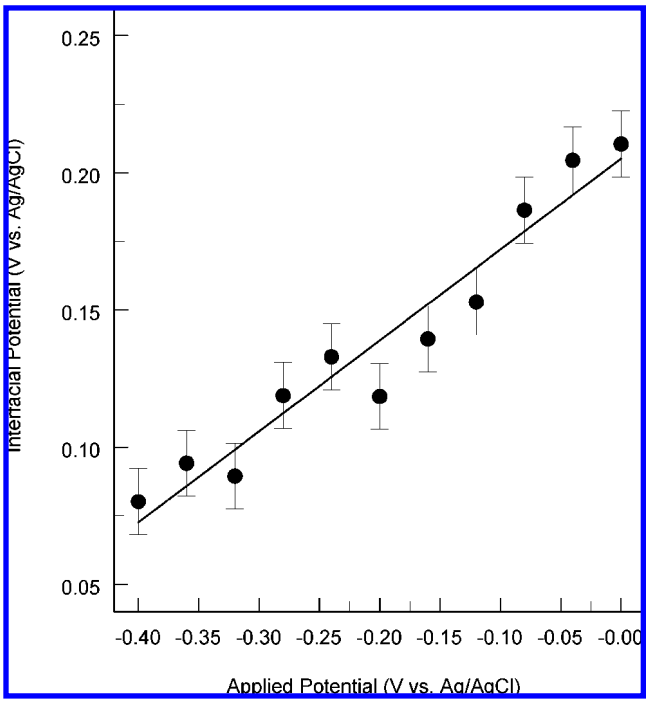

Figure 8. Electrostatic potential at the SHQ/solution interface, φ, determined from the fit of data in Figure 5 to eq 4, plotted versus applied potential.

(d)[44]). Mulliken charge maps of the hydroxyquinoline and keto−hydrazone electron densities on the ring nitrogen and oxygen for both tautomeric forms and the phenolic hydrogen for the azo−quinoline form were equivalent within 0.3% for the two silane- versus thiol-immobilized ligands. Similarities in the vibrational frequencies and intensities of the quinoline ring, azo group, and hydrazone features of the Raman spectra of the two ligands further support the similarity of their electronic structures. Apparently, substituting a silane-coupling group for a thiol makes a negligible difference in the acid−base and metal ion binding properties at the quinoline ring, which is separated by an aromatic ring and azo linkage from the site of immobilization.

To complete the fit of the Cu^{2+}-dependent data to eq 4, one must account for the polarization of the electrode surface by the applied potential. The interfacial activity of Cu^{2+} and H^+ are modified by the potential, φ, at the ligand/solution interface, where $a_{Cu^{2+}} = [Cu^{2+}] \exp(-2F\varphi/RT)$ and $a_{H^+} = [H^+] \exp(-F\varphi/RT)$. These expressions are substituted for $a_{Cu^{2+}}$ and a_{H^+} in eq 4, and only the values of φ and K_{taut} are varied to achieve a least-squares fit between the model and the experimental data. An example is shown in Figure 7 for data acquired at an applied potential of −0.2 V (vs Ag/AgCl), where a fit of the [Cu^{2+}]-dependent speciation provides estimated values of the interface potential, $\varphi = 0.12 \pm 0.01$ V, and the tautomerization equilibrium constant, $K_{taut} = 0.76 \pm 0.04$. The consistent fit of the data to eq 4 validates the model where Cu^{2+} binds to single SHQ ligands in the azo−quinoline form; based on the geometry of surface immobilization, no metal ion bridging complexes are expected to form.[36,37] Note that the effect of the positive interface potential on the local activity of Cu^{2+} is quite significant; for the example in Figure 7, the value of $\varphi = 0.12$ lowers the interfacial activity of Cu^{2+} relative to the bulk concentration by nearly 2 orders of magnitude, $\exp(-2F\varphi/RT) = 0.017$. The fitting procedure above was successfully repeated for all the [Cu^{2+}]-dependent speciation data in Figure 5, for each of the applied potentials from −0.4 to 0.0 V (vs Ag/AgCl). The results of this analysis provide insight into how the interface potential and tautomerization equilibrium vary with changes in applied potential.

In Figure 8, the interfacial potential, φ, estimated from its effect on the activity of Cu^{2+} at the hydroxyquinoline ligand/solution boundary, is plotted versus the potential applied to the electrode with respect to solution. The resulting plot is linear, with a slope of 0.33 ± 0.01 and an *x*-axis intercept of −0.62 ± 0.05 V. The linearity of the plot indicates that the potential at the ligand/solution interface varies in proportion to the applied potential, while the fractional slope indicates that only a fraction of the total applied potential exists between the ligand boundary (where Cu^{2+} binds) and bulk solution. These results show, therefore, that a large fraction (67%) of the applied potential drops across the immobilized ligand. This behavior is consistent with the model of Smith and White for the potential distribution across interfacial films containing acid/base groups.[45] This model predicts that self-assembled monolayers on polarized surfaces experience a greater voltage drop across the film compared to the double layer in the adjacent solution, due to the small capacitance of the film in series with the larger capacitance of the double layer.

The *x*-axis intercept, extrapolated from the linear fit of the data in Figure 8, is the applied potential at which the interface potential

(42) Mukherjee, K. M.; Misra, T. N. *J. Raman Spectrosc.* **1996**, *27*, 595.
(43) Morgan, J. K. *J. Chem. Soc.* **1961**, *part 4*, 2151.
(44) Frisch, M. J.; Trucks, G. W.; Schlegel H. B.; et al. GAUSSIAN 98, Revision A.7, Gaussian Inc., Pittsburgh, PA, 1998.
(45) Smith, C. P.; White, H. S. *Langmuir* **1993**, *9*, 1−3.

vanishes. This result corresponds to the potential of zero charge, PZC = −0.62 ± 0.05 V (vs Ag/AgCl), of the SHQ-modified Ag surface. This is a reasonable result in light of capacitance measurements of the PZC of bare Ag surfaces in contact with aqueous perchlorate solutions, which range from −0.74 to −0.99 V (vs Ag/AgCl),[46−48] depending on the predominant crystal face of surface. The addition of a self-assembled monolayer to the metal surface can also lead to shifts in the PZC, depending on the electronic interactions and charge state of the immobilized ligand.[49] The PZC estimated from the results in Figure 8 is, therefore, a reasonable value for a ligand-modified silver surface and is important in the modeling of electric-field effects on the ligand, as discussed in the following section.

Electrical Control over Tautomerization and Metal Ion Binding. From the above results, it is clear that the applied potential governs the local activity of copper ion at the ligand/solution interface, which influences the complexation equilibrium. In addition, the tautomeric equilibrium (eq 1, above) is shifted by applied potential due to the influence of the local field on the immobilized ligand. Some shifting of the tautomer population arises from increases in the interfacial pH at more positive potentials ($a_{H^+} = [H^+] \exp(-F\varphi/RT)$ and subsequent deprotonation of the azo−quinoline form of the ligand (eq 2). Based on the fitting of the Cu^{2+}-dependent data in Figure 7, this effect accounts for only a ∼2% change in the azo−quinoline population while the tautomerization equilibrium has been switched to be $K_{taut} = 0.76$ in favor of the azo−quinoline form.

The sensitivity of the tautomerization equilibrium to applied potential is demonstrated in Figure 9, where the log of the equilibrium constant, $\ln(K_{taut})$, determined from fitting the tautomer fraction data in Figure 5 to eq 4, is plotted versus applied potential. The log of the tautomerization equilibrium is found to vary linearly with the applied potential, which is likely due to the influence of the large electric field on the electronic structure of the immobilized ligand. Recall that the potential at the ligand/solution interface is a fraction of the total applied potential (see above), which indicates that there is a large voltage drop across the immobilized ligand. The resulting electric field from this voltage drop could influence the structure of the ligand, analogous to electric-field induced isomerization of immobilized ligands recently reported.[3,4] In the present case, the electrical control may originate from the stabilization of one tautomeric form over another by the electric field, due to differences in the dipole moments of the two tautomeric forms. To test this possibility, the electric dipole moment of each tautomer was calculated using density functional theory (B3LYP 6-31G(d)[44]). The results of these electronic structure calculations show that there is, indeed, a large difference in the dipole moment of the tautomers: the keto−hydrazone form exhibits a large dipole moment of 5.8 D, while that of the azo−quinoline form is ∼7 times smaller, 0.8 D, both oriented away from the site of immobilization, as illustrated in Figure 10. The applied potentials in these experiments are all more positive than the PZC (−0.62 V, see above) and, accordingly, the large dipole moment of the keto−hydrazone tautomer would be destabilized at large positive potentials. This model is consistent with the switching of the ligand to the less dipolar, enol−azo form at positive potentials. The free energy of a dipole, μ, in an electric field, ϵ, is the dot product, $\mu\cdot\epsilon$, so that the free energy difference between the two tautomers can be estimated from the dot product of the difference in electric dipole moment, $\Delta\mu$, and the electric field, ϵ, across the SHQ monolayer.

$$\Delta G_{taut} = \Delta G^{o}_{taut} + \epsilon\cdot\Delta\mu \qquad (5)$$

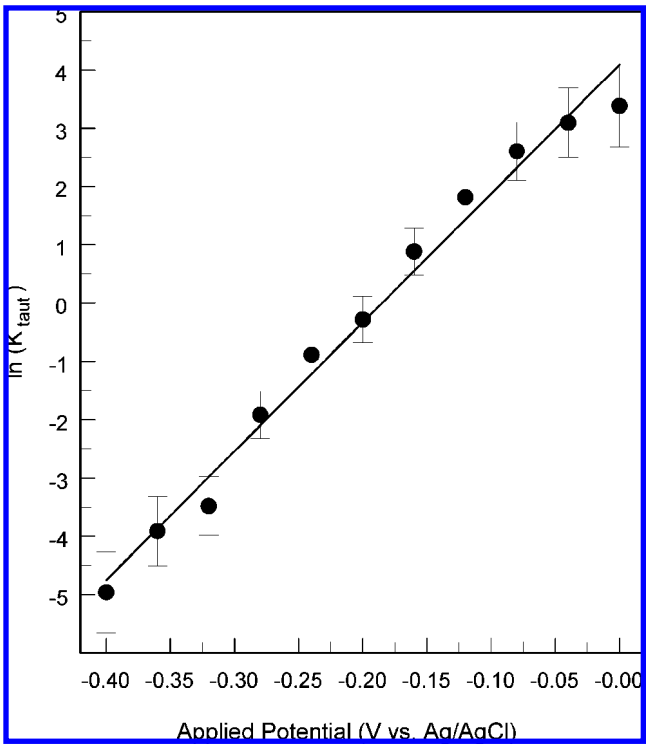

Figure 9. Logarithm of the tautomerization equilibrium constant, K_{taut}, determined from the fit of data in Figure 5 to eq 4, plotted versus applied potential.

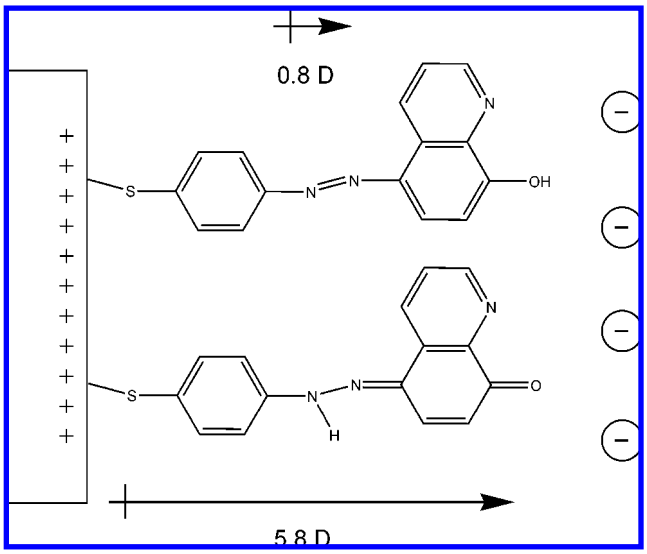

Figure 10. Direction and magnitude of the permanent electronic dipole moments of both tautomeric forms of SHQ estimated by density functional theory calculations.

(46) Valette, G. *J. Electroanal. Chem.* **1981**, *122*, 285.
(47) Valette, G.; Hamelin, A. *J. Electroanal. Chem.* **1982**, *131*, 229.
(48) Larkin, D.; Guyer, K. L.; Hupp, J. T.; Weaver, M. J. *J. Electroanal. Chem.* **1982**, *138*, 401.
(49) Iwami, Y.; Hobara, D.; Yamamoto, M.; Kakiuchi, T. *J. Electroanal. Chem.* **2004**, *564*, 77−83.

where ΔG^{o}_{taut} is the free energy difference between the immobilized tautomers at the PZC. Because the tautomerization equilibrium constant depends exponentially on the free energy difference, $K^{o}_{taut} = \exp(-\Delta G^{o}_{taut}/RT)$, the tautomerization equilibrium constant will depend exponentially on the electric field across the ligand:

$$K_{taut} = K^{o}_{taut} \exp(+\epsilon \cdot \Delta\mu/kT) \quad (6)$$

The electric field should be proportional to the voltage drop across the ligand, which is a constant fraction (~67%) of the applied potential, according to the results in Figure 8. Thus, eq 6 predicts the behavior exhibited by the ligand in Figure 9, where the log of the tautomerization equilibrium constant varies linearly with applied potential and the slope is: $\Delta\mu \cdot \epsilon/kT$ (E_{app} − PZC). The value of ln (K^{o}_{taut}) = −9.6 was determined by extrapolating the linear response in Figure 9 to E_{app} = PZC (−0.62 V). This provides an estimate of free energy difference between the keto−hydrazone tautomer and the enol−azo form in the absence of an external electric field: $RT \ln(K^{o}_{taut}) = \Delta G^{o}_{taut} \sim +24$ kJ/mol, where the enol−azo tautomer is less stable than keto−hydrazone form. The field-free equilibrium imbalance in favor of the strongly dipolar keto−hydrazone tautomer is consistent with similar systems. For example, 2-pyridone is favored by 16−19 kJ/mol in water or polar solvents over its cognate tautomer, 2-hydroxypyridine, the latter being more stable in low dielectric environments.[50,51]

The magnitude of electric field across the ligand, ϵ, required to switch to the enol−azo form can be estimated from eq 6 and least-squares fit of the data in Figure 9. From these results, $\ln(K_{taut}) = 0$ at an applied potential, $E_{app} = -0.185$ V, where $-\ln(K^{o}_{taut}) = 9.6 = \Delta\mu \cdot \epsilon/kT$. Using the value of $\Delta\mu \sim 5.0$ D from DFT calculations and assuming the ligand dipole is oriented away from the electrode surface predicts the magnitude of the electric field required to switch the ligand, $\epsilon \sim 2.3 \times 10^{9}$ V m^{-1}. This result should be considered an upper bound because any tilting of the ligand from the surface normal, $\theta = 0$, would reduce the field along the axis of the ligand; the dependence of the dot product, $\Delta\mu \cdot \epsilon$, on tilt angle is cos θ, which varies slowly near $\theta = 0$. The electric field predicted to switch the SHQ ligand is comparable to the interfacial electric field, $\epsilon \sim 2.5 \times 10^{9}$ V m^{-1}, measured at a ligand/solution interface by the vibrational Stark shift of a nitrile-terminated alkanethiol monolayers immobilized on polished Ag electrodes.[52,53] While the structures of these self-assembled monolayers are different (a conjugated aromatic thiol versus a nitrile-terminated *n*-alkanethiol), the ligands appear to experience comparable interfacial electric fields at polarized silver surfaces.

To further test the influence of interfacial dielectric environment on the relative stability of the two tautomers, the potential dependence of the SERS spectra of mixed monolayers composed of SHQ diluted into other thiol molecules was investigated. Two mixed monolayers were studied, mercaptohexanol with SHQ and *n*-heptanethiol with SHQ, to approximate intermediate and low dielectric environments, respectively. The heptanethiol mixed monolayers should have the most hydrophobic character and should exclude water and ions.[54] Accordingly, one would expect that a lower dielectric environment would destabilize the polar keto−hydrazone tautomer relative to the enol−azo form. This predicted behavior was indeed observed in the experimental data, shown in Figure 11, in which SERS spectra of SHQ/heptanethiol monolayers exhibit little evidence of the keto−hydrazone tautomer, except at the most negative applied potentials. The mixed mercaptohexanol film, due to the pendant hydroxyl moiety, should allow some water and counterions to penetrate into the film to create a higher dielectric constant environment, where the dipolarity of the keto−hydrazone form could be partially stabilized. SERS spectra of mercaptohexanol/SHQ monolayers show that the relative population of the enol−azo tautomer appears with small positive potentials relative to the PZC, but the response is spread out over a wide potential range, indicating a less homogeneous environment compared to a pure SHQ layer, perhaps due to nonuniform mixing of the two ligands.[55] The polarizability, dipolarity, and uniformity of the pure SHQ layer is likely greater than either of the mixed monolayers. These attributes of the pure SHQ monolayer contribute to the greater stability of the keto−hydrazone tautomer and the uniform and sharp potential dependence for tautomer switching of this film.

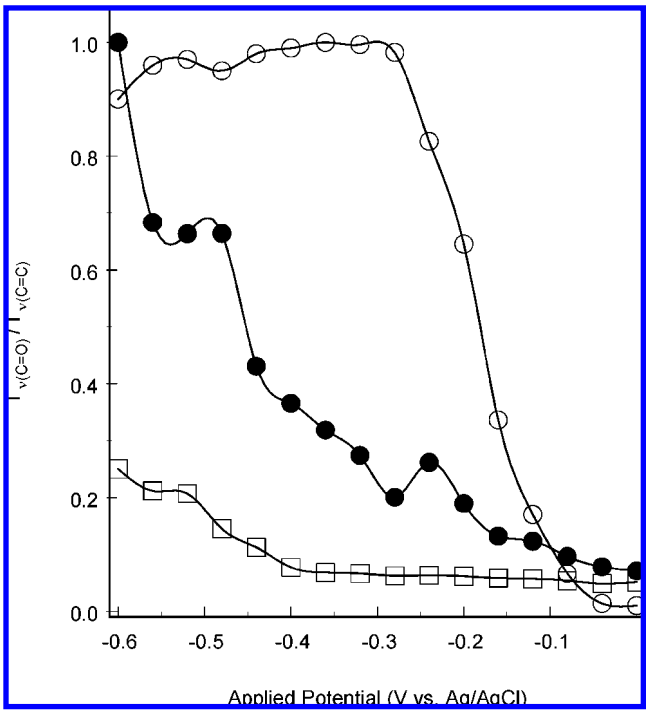

Figure 11. Relative population of keto−hydrazone tautomer of immobilized SHQ ($I_{\nu(C=O)}/I_{\nu(C=C)}$) as a function of applied potential (V vs Ag/AgCl) as a function of monolayer composition. Ag surfaces functionalized from ethanolic solutions containing 1 mM SHQ (open circles); 7:1 1 mM mercaptohexanol/1 mM SHQ (closed circles); 2:1 1 mM heptanethiol/1 mM SHQ (open squares).

CONCLUSIONS

SERS-based spectroelectrochemical measurements have revealed that the tautomerization equilibrium of SHQ immobilized

(50) Frank, J.; Katritzky, A. R. *J. Chem. Soc., Perkin Trans. 2* **1976**, 1428.
(51) Issacs, N. S. *Physical Organic Chemistry*; Longham: Essex, 1987; Chapter 5.
(52) Oklejas, V.; Sjostrom, C.; Harris, J. M *J. Am. Chem. Soc.* **2002**, *124*, 2408.
(53) Oklejas, V.; Sjostrom, C.; Harris, J. M *J. Phys. Chem. B* **2003**, *107*, 7788.
(54) Poirier, G. E.; Pylant, E. D.; White, J. M. *J. Chem. Phys.* **1996**, *105*, 2089.
(55) Oklejas, V.; Harris, J. M. *Langmuir* **2003**, *19*, 5794.

at Ag surfaces is controlled by the applied potential. The observed potential dependence is striking: a change in applied potential less than 300 mV results in nearly complete switching of the relative population of immobilized tautomeric species, from the keto−hydrazone to the enol−azo form. Subsequent experiments demonstrate that immobilized SHQ complexes Cu^{2+} and that the complexation equilibrium, coupled to the tautomerization equilibrium, can be controlled through the applied potential. Thus, a small change in potential can be used to spontaneously "switch" the favored immobilized tautomer and inhibit the ability of immobilized SHQ to bind Cu^{2+}, which binds preferentially to the enol−azo species.

The mechanism for the observed potential dependence is correlated with the structure of the interfacial environment and the apparent strength of interfacial electric fields that are a result of interfacial structure. The data suggest that monolayers composed of SHQ support large electric fields that influence the tautomerization equilibrium through the interaction of dipole moments of the two tautomers with the interfacial electric field. The effect of $[Cu^{2+}]$ on the potential dependence of SHQ monolayers was also studied and used to estimate the potentials at the ligand/solution interface, which are consistent with a significant voltage drop across the ligand. The results suggest a new paradigm for electrical control over interfacial reactions: tautomerization of immobilized species offers a facile method for introducing molecular and electronic structural differences that can be exploited to produce an electrically "switchable" surface. This work also demonstrates that surface-enhanced Raman spectroscopy provides critical insight into the interfacial phenomena and structures that govern the potential-dependent response.

ACKNOWLEDGMENT

The authors thank those who contributed significantly to this study: Tom Beebe and his student Matt Wells at the University of Delaware for acquisition of XPS data, Henry White and his students Chett Boxley and John Watkins, for production of annealed Ag films on mica and acquisition of cyclic voltammograms of SHQ-modified Ag electrodes, respectively. This research was supported in part by the U.S. Department of Energy under Grant DE-FG03-93ER14333.

SUPPORTING INFORMATION AVAILABLE

Additional information as noted in text. This material is available free of charge via the Internet at http://pubs.acs.org.

Received for review August 27, 2007. Accepted December 13, 2007.

AC701808Z